TÜBİTAK

Turkish Journal of Chemistry

http://journals.tubitak.gov.tr/chem/

Research Article

Turk J Chem
(2017) 41: 826 – 844
© TÜBİTAK
doi:10.3906/kim-1612-25

Cyclic voltammetry behavior of tamoxifen in different electrolytes, electrochemical characterization, and its measurement by differential pulse anodic voltammetry

Zeinab DERIS FALAHIEH, Mehdi JALALI*, Mohammad ALIMORADI
Department of Chemistry, Faculty of Science, Islamic Azad University, Arak branch, Arak, Iran

Received: 09.12.2016 • **Accepted/Published Online:** 08.05.2017 • **Final Version:** 20.12.2017

Abstract: Cyclic voltammetry (CV) was performed on tamoxifen (tam) using different electrodes and in various acidic electrolytes containing 10% v v^{-1} methanol (MeOH). Tam oxidation was found to be most favorable using 0.1 mol L^{-1} H_2SO_4. To investigate the mechanism, we performed chronoamperometry, CV at different scan rates, differential pulse anodic voltammetry (DPAV), and electrochemical impedance spectroscopy on tam-covered glassy carbon electrodes (GCEs). The electrode area, diffusion coefficient, and surface concentration (Γ) of tam were calculated to be 0.062 cm^2, 3.65 $\times$ 10^{-6} cm^2 s^{-1}, and 3.2 $\times$ 10^{-10} mol cm^{-2} respectively. Then the effects of different parameters on the DPAV were optimized. The best conditions were 2.5% v v^{-1} cMeOH, 0.1 mol L^{-1} H_2SO_4, deposition potential 0.4 V, deposition time 30 s, and GCE rotating rate 400 rpm. Therefore, the calibration curve was plotted in the range of 0.5 to 5 μg mL^{-1}. The limits of detection and quantitation (LOD and LOQ) were found to be 0.008 and 0.025 μg mL^{-1}, respectively. The relative bias and standard deviation of 2 μg mL^{-1} tam were estimated to be 5% (n = 5) and 2.3%, respectively. Finally, the proposed method was successfully employed for the determination of tam in real samples.

Key words: Tamoxifen, differential pulse anodic voltammetry, glass carbon electrodes, serum analysis

1. Introduction

Tamoxifen (tam) is a medication that was discovered in 1967; it is recommended for preventing breast cancer in women and for the treatment of hormone-sensitive breast cancer in both women and men.[1] This medication is an estrogen antagonist and can bond to estrogen receptors and suppress the growth of breast tumors. It is metabolized in the liver by enzymes, including CYP2D6 and CYP3A4. The resulting metabolites, 4-hydroxy tam (afimoxifene) and N-desmethyl-4-hydroxytamoxifen (endoxifen), have 30 to 100 times more affinity for estrogen receptors than that of tam alone.[2] However, tam and its metabolites block growth factor proteins in breast tissue.[3] Then this complex inhibits the effects of estrogen and suppresses the DNA synthesis in cell proliferation.[4–7]

Different analytical methods have been developed to investigate and determine tam and its metabolites in biological and pharmaceutical products. One of the major steps in obtaining a drug certificate is completing an analytical study. Analytical techniques, such as spectrophotometry,[8–12] Fourier transform infrared spectroscopy,[13,14] high-performance liquid chromatography,[15,16] gas chromatography,[17,18] ion chromatography,[19,20] capillary electrophoresis,[21–26] fluorescence and phosphorescence methods[27–30], and elec-

*Correspondence: jalalimehdian@yahoo.com

trochemical methods, such as polarography,[31] cyclic voltammetry (CV),[32] differential pulse voltammetry,[33] and amperometry,[34] have been used to analyze and control the dosage of tam in different samples. Among these methods, electrochemical techniques have some advantages, including simplicity, low cost, and fast speed. These methods can provide valuable parameters, such as the diffusion coefficient, a kinetic constant, a stability coefficient, and the number of electrons contributing to the electrode reactions. Valuable pharmacology information on some anticancer drugs can be obtained through electrochemical techniques. The action mechanism, intermediate detection, and side effects of an anticancer drug can be investigated through different electrochemical experiments. Research on anticancer drugs demonstrates that most of these types of medications have electroactive groups, such as OH and NH_2. Thus, the electroanalytical signals of these drugs can be attributed to the oxidation of these functional groups or oxidative cyclization reactions.[35] Consequently, electrochemical techniques have attracted significant attention in the analysis of these drugs due to their low detection limits and their speed. The DPAV behavior of tam on glass carbon electrodes (GCEs) in B-R buffer has shown significant oxidation peaks.[35] These peaks were also observed in carbon-paste electrodes.[36] Therefore, some researchers have attributed these peaks to the cyclization reactions of tam.[35–37]

The aim of this study was to find sufficient electrolytes and electrodes in order to diminish the effects of the phenomena limiting counter and working electrode reactions during tam oxidation. The major goal of this research was to enhance the current peak of tam oxidation, as previously reported.[35] Therefore, the voltammetry behavior of tam in different electrolytes, such as B-R buffer, H_2SO_4, HCl, H_3PO_4, and CH_3COOH on the surfaces of solid-state electrodes, such as Pt, Au, GCE, and multiwall carbon nanotubes (MWCNTs) paste electrode, were investigated. Chronoamperometry, cyclic voltammetry, and EIS were performed to show the process that contributes to the tam oxidation reactions, and a simple, sensitive, and cheap DPAV was used to obtain a novel methodology for the determination of tam in different samples using electrolyte-assisted signal enhancement. Finally, the proposed method was used to test the content of tam in pharmaceutical products and in blood serum samples.

2. Results and discussion

2.1. Cyclic voltammetry

In the first experiment, the CV of tam in different electrolytes, such as CH_3COOH (Figure 1a), H_3PO_4 (Figure 1b), B-R buffer (Figure 1c), HNO_3 (Figure 1d), and H_2SO_4 (Figure 1e) on GCEs was recorded. As can be seen, an irreversible peak centered at about 1 V appeared in different electrolytes. This peak is attributed to the electrochemical cyclization reactions of tam (Scheme).[37] The cyclization reactions of tam that take place in an anodic sweep produces 2 mol of protons per 1 mol of tam. However, the presence of an excess amount of H^+ ions not only enhances hydrogen evolution at the auxiliary electrode but also suppresses tam cyclization and decreases the current peak related to the reaction. The obtained results show that the sharpest peak was achieved in 0.1 mol L^{-1} H_2SO_4. Therefore, H_2SO_4 (as a strong acid) diminishes the resistance of electrochemical media and subsequently enhances the total current of the electrochemical circuit. It is valuable to note that the presence of H^+ ions can affect the total current positively or negatively. Thus, the H^+ concentration must be adjusted to achieve minimum electrochemical resistance against the total current. In addition, the peak height decreases with increasing pKa ($K_{CH3COOH} = 1.75 \times 10^{-5}$ and $K_{1H3PO4} = 7.11 \times 10^{-3}$). Compared with 0.1 mol L^{-1} H_2SO_4, 0.2 mol L^{-1} HNO_3 caused the peak current to decrease and to shift to less positive potential due to the oxidative nature of NO_3^- ions in acidic media.

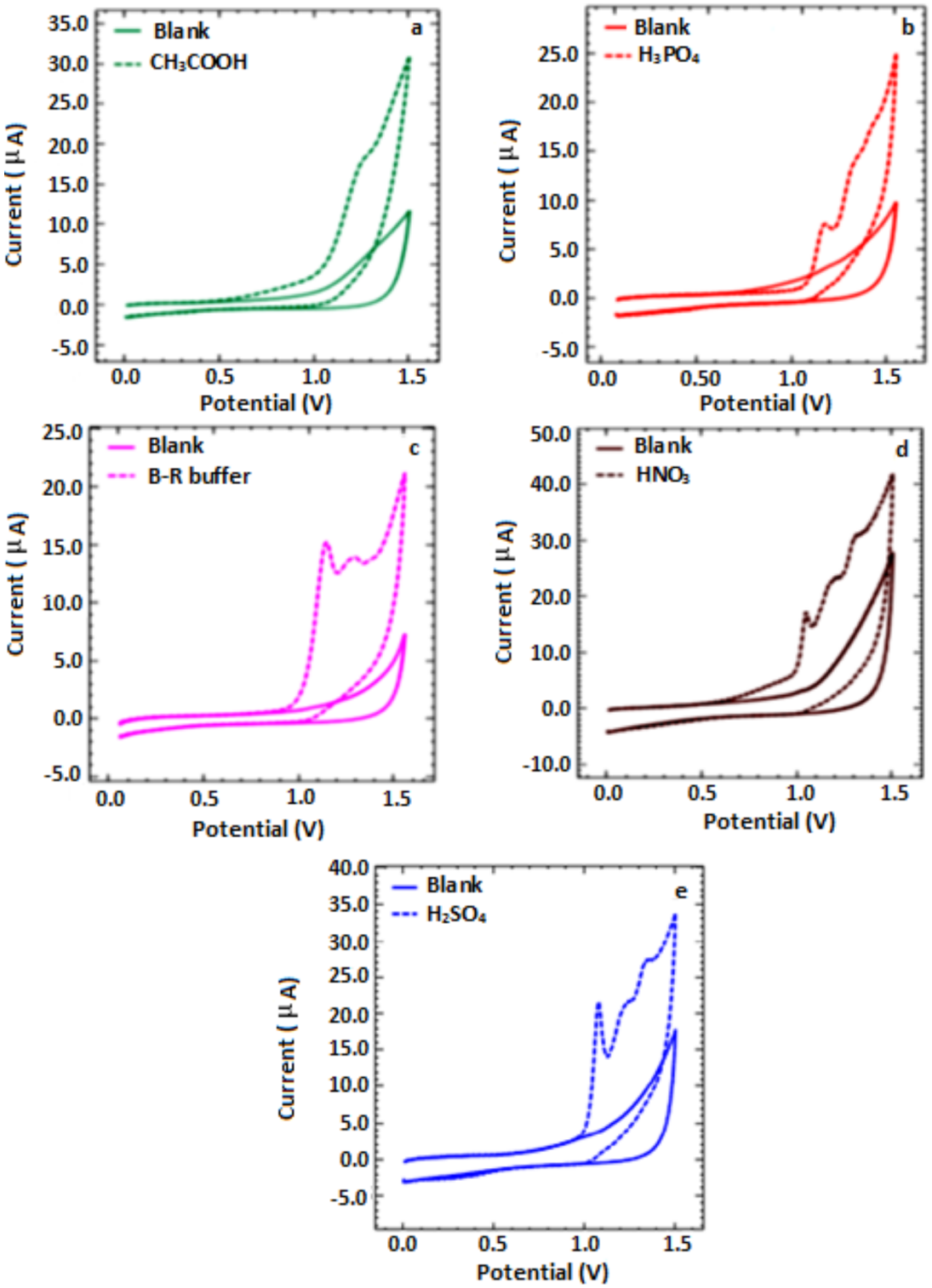

Figure 1. CV of 5 μg mL^{-1} tam on the GCE in 0.2 mol L^{-1} CH_3COOH:10% v v^{-1} MeOH (a) 0.1 mol L^{-1} H_3PO_4:10% v v^{-1} MeOH (b), B-R buffer pH 4.2:10% v v^{-1} MeOH (c), 0.2 mol L^{-1} HNO_3:10% v v^{-1} MeOH (d), and 0.1 mol L^{-1} H_2SO_4:10% v v^{-1} MeOH (e). Scan rate = 100 mV s^{-1}.

To predict the electrochemical behavior of Tam in H_2SO_4 on different solid-state electrodes, the CVs were also recorded on the Au (Figure 2a), Pt (Figure 2b), MWCNT paste (Figure 2c), and MWCNT-GC (Figure 2d) electrodes. As seen, no considerable peak appeared on the other electrodes compared to the bare GCE (Figure 2e). Pt and Au electrodes are sufficient for evolving oxygen gas via H_2O oxidation. To increase the electrochemical surface of the GCE, the bare GCE was modified by MWCNTs. On the surface of MWCNT-GCE, the oxidation peak attributed to tam disappeared due to the strong adsorption of tam on the MWCNT-GCE compared to the bare GCE.[38] Hence, 0.1 mol L^{-1} H_2SO_4 and the bare GCE were chosen as the best electrode and electrolyte, respectively, for performing the following experiments.

2.2. Mechanistic studies

2.2.1. Chronoamperometry

One useful electrochemical technique for finding the electrochemical surface area and diffusion coefficient of an analyte is chronoamperometry. In this technique, the working electrode surface is excited by a potential step, and the faradic current caused by the transfer of electrons changes with respect to time, as described in the Cottrell equation as follows:

$$i = nFAC_j^* D_j^{1/2} \pi^{-1/2} t^{-1/2}, \quad (1)$$

where i is the current in unit A, n is the number of electrons per molecule that contributes to an electron transfer event, F is the Faraday constant (i.e. 96485 C mol^{-1}), A is the area of the electrode surface in cm^2, C_j^* is the bulk concentration of analyte in mol cm^{-3}, D_j is the diffusion coefficient for species j in cm^2 s^{-1}, and t is the time in seconds.

To simplify the equation, the constants (i.e. n, F, A, C_j^*, and D_j) are collected in K. Therefore, the equation is rewritten as follows to achieve good linearity between 2 and 10 s:

$$i = Kt^{-1/2} \quad (2)$$

In this investigation, $K_4Fe(CN)_6$ was first used as a probe to determine the electrochemical surface area; its diffusion coefficient was 6×10^{-6} cm^2 s^{-1}. To find the electrochemical surface area, different concentrations of $K_4Fe(CN)_6$, including 0.5, 1, 5, and 10 mmol L^{-1}, were tested, and different chronoamperograms were recorded (Figure 3a). The Cottrell plots (i vs $t^{-1/2}$) are also plotted (Figure 3b), and their slopes versus the $K_4Fe(CN)_6$ concentration are highlighted (Figure 3c). As defined previously, the collected K was a function of $[K_4Fe(CN)_6]$, and its slope was equal to $FAC_j^* D_j^{1/2} \pi^{-1/2}$. Therefore, the electrochemical surface area (A) was calculated to be 0.062 cm^2. However, the electrochemical characteristics of the GCE (OD = 3 mm) were close to the geometrical surface area of the electrode ($\sim$ 0.07 cm^2). The final goal of this investigation was to determine the diffusion coefficient of the tam analyte. Hence, two concentrations of tam were chosen: 3 and 6 mmol L^{-1} in 0.1 mol L^{-1} H_2SO_4:10% v v^{-1} MeOH. After that, the chronoamperometry experiments were conducted. The plots of i versus t (Figure 4a) and i versus $t^{-1/2}$ (Figure 4b) were recorded, and the average diffusion coefficient of tam was found to be 3.65×10^{-6} cm^2 s^{-1}.

2.2.2. Voltammetric observations

To investigate the processes contributing to the electrode's reactions, the influence of the scan rate on the cyclic voltammograms (Figure 5a) was studied, as useful electrochemical information can be obtained from

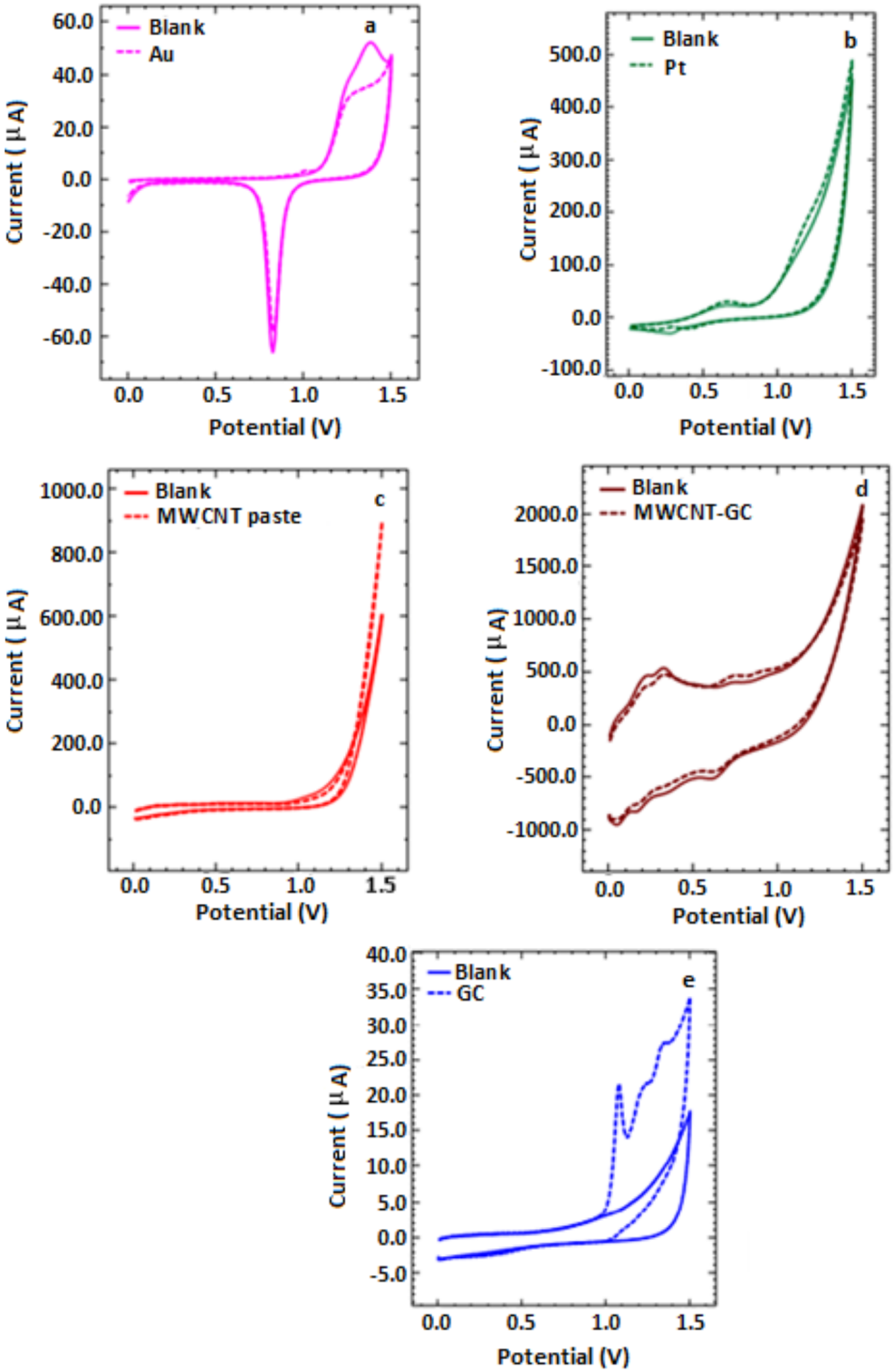

Figure 2. CV of 5 μg mL^{-1} tam in 0.1 mol L^{-1} H_2SO_4:10% v v^{-1} MeOH (as blank solution) on Au (a), Pt (b), MWCNT paste(c), MWCNT-GC (d), and GC electrode (e). Scan rate = 100 mV s^{-1}.

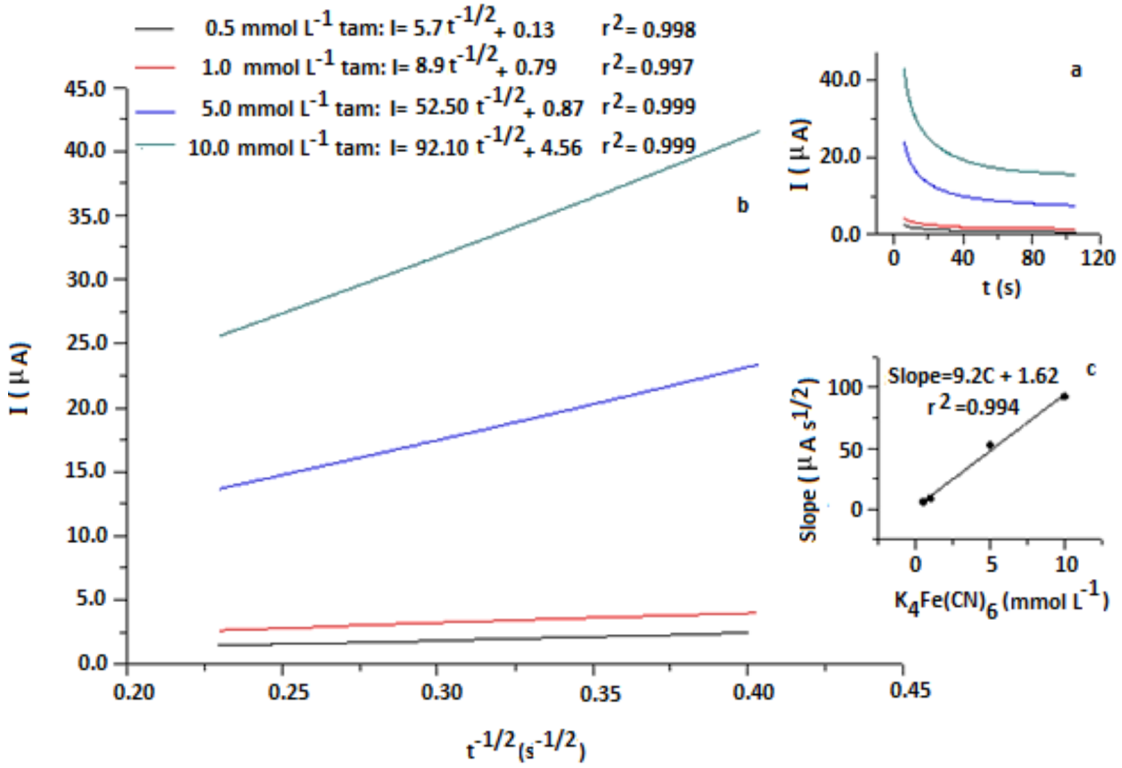

Figure 3. Chronoamperometry curves of $[K_4Fe(CN)_6]$. i versus t (a), i versus $t^{-1/2}$ (b) and slope of i- $t^{-1/2}$ versus $[K_4Fe(CN)_6]$ (c). Potential step 0.3 V, recording time 100 s, and interval time 0.01 s.

the relationship between the peak current and the scan rate. Studies of the scan rate (ν) were carried out to demonstrate whether the reaction on a GCE is diffusion or adsorption controlled. The effects of ν (mV s^{-1}) and $\sqrt{\nu}$ (mV $s^{-1})^{1/2}$ on the peak current are shown in Figures 5b and 5c, respectively. As seen in Figure 5b, the effect of the scan rate on the oxidation peak current showed a better linear relation at a rate of 25 to 300 mV s^{-1}. Therefore, the kinetics of tam oxidation on the GCE in 0.1 mol L^{-1} H_2SO_4:10% v v^{-1} MeOH were controlled by the adsorption process. As shown in Figure 5b, the linear equation is expressed as follows:

$$I_P = 0.0744\nu + 1.3713, \tag{3}$$

which is based on Laviron's equation as follows:[39]

$$I_P = n^2F^2\nu A\Gamma/4RT, \tag{4}$$

where A (= 0.062 cm^2 obtained from chronoamperometry) is the area of used GCE, n (= 2) is the number of electrons per one mole of tam, F is the Faraday constant, ν (mV s^{-1}) is the scan rate, R is the gas constant, and T is the thermodynamic temperature. The slope of I_P versus ν was used to find the surface concentration (Γ) of the analyte. The Γ value was calculated to be 3.2 $\times$ 10^{-10} mol cm^{-2}. This amount of surface concentration is very close to the other component adsorbed on the GCE before charge transfer.[40]

A DPAV investigation was also carried out to emphasize the contribution of the surface phenomena in this reaction. In the first step of this study, the electrochemical circuit was open and the rotation rate was 400 rpm (120 s). Tam was self-accumulated on the surface of the GCE from the 0.1 mol L^{-1} H_2SO_4:10%

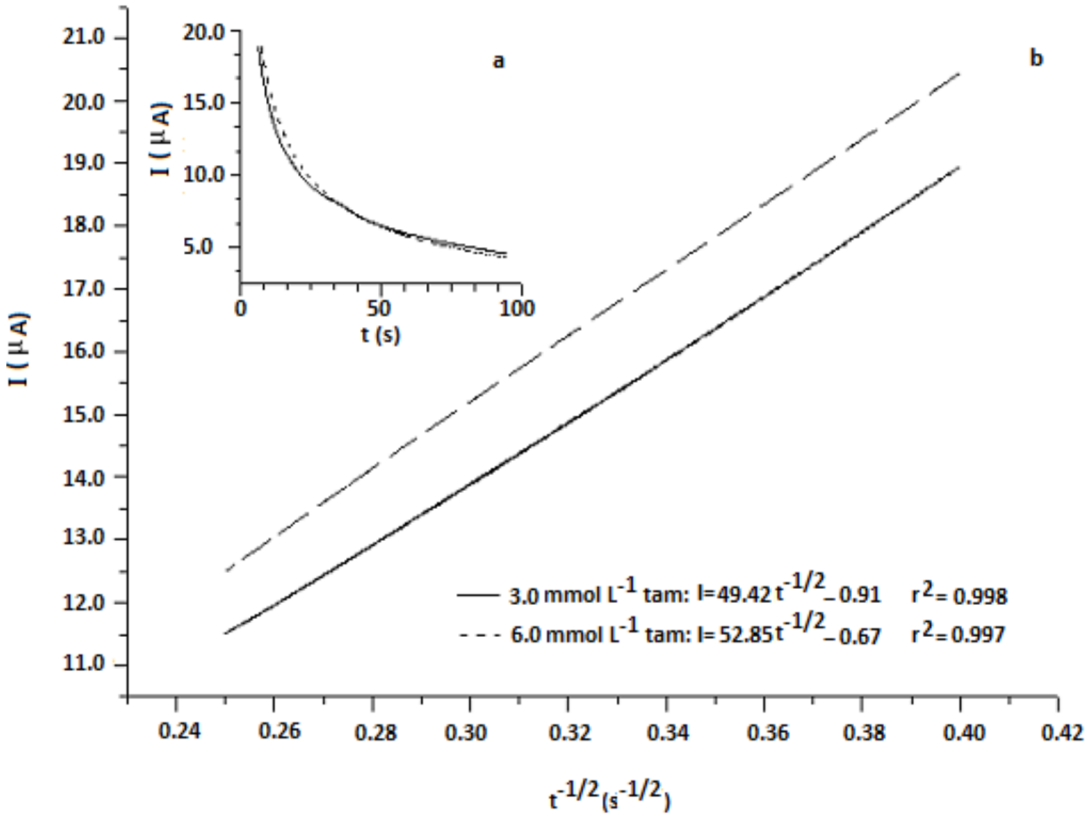

Figure 4. Chronoamperometry plots of tam. i versus t (a) and i versus $t^{-1/2}$ (b). Potential step 1.1 V, recording time 100 s, and interval time 0.01 s.

v v^{-1} MeOH solution (i.e. the blank sample) containing 5 μg mL^{-1} tam. Then the tam-covered GCE was rinsed with double-distilled water, and the DPAV was recorded in fresh 0.1 mol L^{-1} H_2SO_4:10% v v^{-1} MeOH. In the second step, a tam-covered GCE was prepared via electrochemical deposition at –1.4 V versus the Ag/AgCl reference electrode in a stationary condition (120 s). Subsequently, the DPAV was recorded in the same conditions as the previous one. In the final step, a tam-covered GCE was prepared via electrochemical deposition at 400 rpm for 120 s. The obtained voltammograms are presented in Figure 6. As seen, dynamic self-accumulation and electrochemical deposition both accelerate the adsorption of tam by the GCE surface, as the highest signal for the DPAV of the tam-covered GCE in fresh solution was achieved in these conditions. Therefore, the preconcentration of tam on the surface of the GCE under stirring and after applying cathodic potential can enhance the tam oxidation peak. However, in this study, tam oxidation was extensively controlled by the surface phenomena.

2.2.3. Impedance investigations of the bare GCE and tam-covered GCE

To further interpret the tam and GCE interactions, EIS was carried out. The Nyquist plots of the bare GCE and tam-covered GCE (tam deposited by 120-s electrolysis at –1.4 V and a rotating rate 100 rpm in 0.1 mol L^{-1} H_2SO_4:10% v v^{-1} MeOH in acetate buffer with a pH of 4 (Figures 7a and 7b) and in the 0.2 mol L^{-1} NaOH at the presence of 0.1 mol L^{-1} $[Fe(CN)_6]^{-3/-4}$ (Figure 7c) were recorded at OCP (0.16 V) and 0.25 V, respectively. Their electrochemical responses are different; the shape of a Nyquist plot depends on the

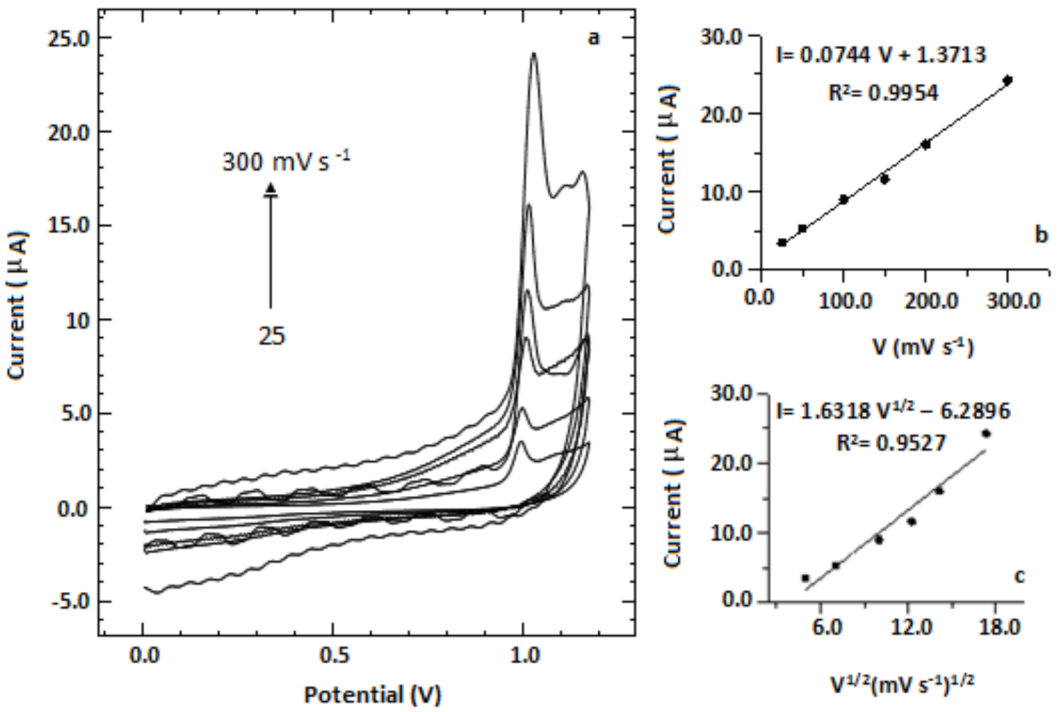

Figure 5. CV of 2 μg mL^{-1} tam in 0.1 mol L^{-1} H_2SO_4:10% v v^{-1} MeOH on GCE at different scan rates (a), the peak height versus the scan rate (b), and the peak height versus the square root of the scan rate and (c).

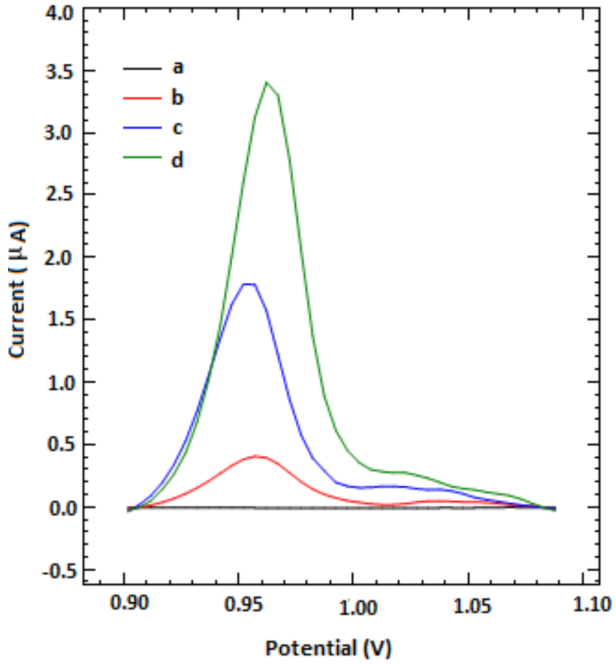

Figure 6. DPAV in fresh 0.1 mol L^{-1} H_2SO_4:10% v v^{-1} MeOH (blank) for the bare GCE (a), and for the tam-covered GCEs prepared from 5 μg mL^{-1} tam in blank; via the self-accumulation under an open circuit and a rotation rate 400 rpm (120 s) (b), via deposition at –1.4 V vs Ag/AgCl and a rotation rate 0 rpm (120 s) (c), and via the deposition at –1.4 V vs Ag/AgCl and a rotation rate 400 rpm (120 s) (d).

electrode's surface properties and the electrolyte medium. As shown in Figure 7b, the tam layer adsorbed on the surface of the GCE caused a slight change in the diameter of the Nyquist semicircle. The smaller semicircle at high frequencies observed for bare GCE suggests fast charge transfer kinetics with respect to the tam-covered GCE. It was also observed that the slope angle of the linear part was closer to 45° for the bare GCE (Figure 7a), which suggests more pronounced diffusion of the acetate buffer bulk electrolyte from the bare GCE surface. It is also clear that the slope angle of the Nyquist linear part for the tam-covered GCE was closer to 90° for the charge consumption event (Figure 7a), as the formation of the tam layer during cathodic deposition prevented diffusion to the GCE surface. To emphasize the change in the interface properties of GCE after the cathodic deposition of tam, the EIS response of the $[Fe(CN)_6]^{-3/-4}$ probe was also recorded in 0.2 mol L^{-1} NaOH (Figure 7c). It is obvious that the Nyquist semicircle's diameter for the bare GCE was smaller than that of the Nyquist semicircle for the tam-covered GCE. Therefore, this investigation indicated the high value of the charge transfer resistance of Fe(III)/Fe(II) in the tam-covered GCE compared to that of the bare GCE. Hence, these EIS observations demonstrate the cathodic adsorption of tam analytes before charge transfer.

2.3. Influence of different parameters on the differential pulse voltammetry current peak

The following experiments were carried out under a tam concentration of 5 μg mL^{-1}, 0.1 mol L^{-1} H_2SO_4, a deposition potential of –1.4 V, a mixing rate of 400 rpm, and a deposition time of 30 s, except when that parameter was under investigation. It is noted that the scan rate 10 mV s^{-1}, pulse amplitude 0.025 V, and pulse interval time 0.5 s were chosen as the DPAV experiment's conditions.

2.3.1. Effects of MeOH

To investigate the effects of MeOH on the current peak of tam oxidation, the MeOH content was varied from 1% to 40% v v^{-1}. As shown in Figure 8, the current peak decreased with increasing MeOH concentrations, as electrolyte conductivity (Figure 8, inset) decreased and the current peak was suppressed. This investigation demonstrated that the highest current peak was obtained by 2.5% v v^{-1} MeOH in 0.1 mol L^{-1} H_2SO_4. Although the presence of MeOH suppressed the peak high, it caused proper dispersion of the tam analyte through the electrolyte, as no significant changes in the electrolyte resistance were achieved compared to 1% v v^{-1} MeOH. Therefore, 0.1 mol L^{-1} H_2SO_4:2.5% v v^{-1} MeOH was chosen for the next experiments.

2.3.2. Effects of H_2SO_4

To investigate the influence of the H^+ ions, DPAV experiments were carried out with different concentration levels of H_2SO_4. As shown in Figure 9, the peak current was increased by increasing the H_2SO_4 concentration from 0.01 to 0.1 mol L^{-1}. This is because, in 0.1 mol L^{-1} H_2SO_4, the resistance against the current flow was less than that in 0.01 mol L^{-1} H_2SO_4. However, when the H_2SO_4 concentration was greater than 0.1 mol L^{-1}, the current peak decreased considerably due to the suppressing effect of the high concentration of the H^+ ions in the cyclization equilibrium. However, with an increasing H^+ ion concentration, the peak potential became less positive due to thermodynamic effects on both working and auxiliary electrode reactions. Hence, 0.1 mol L^{-1} H_2SO_4 was chosen as the best concentration to perform the following experiments.

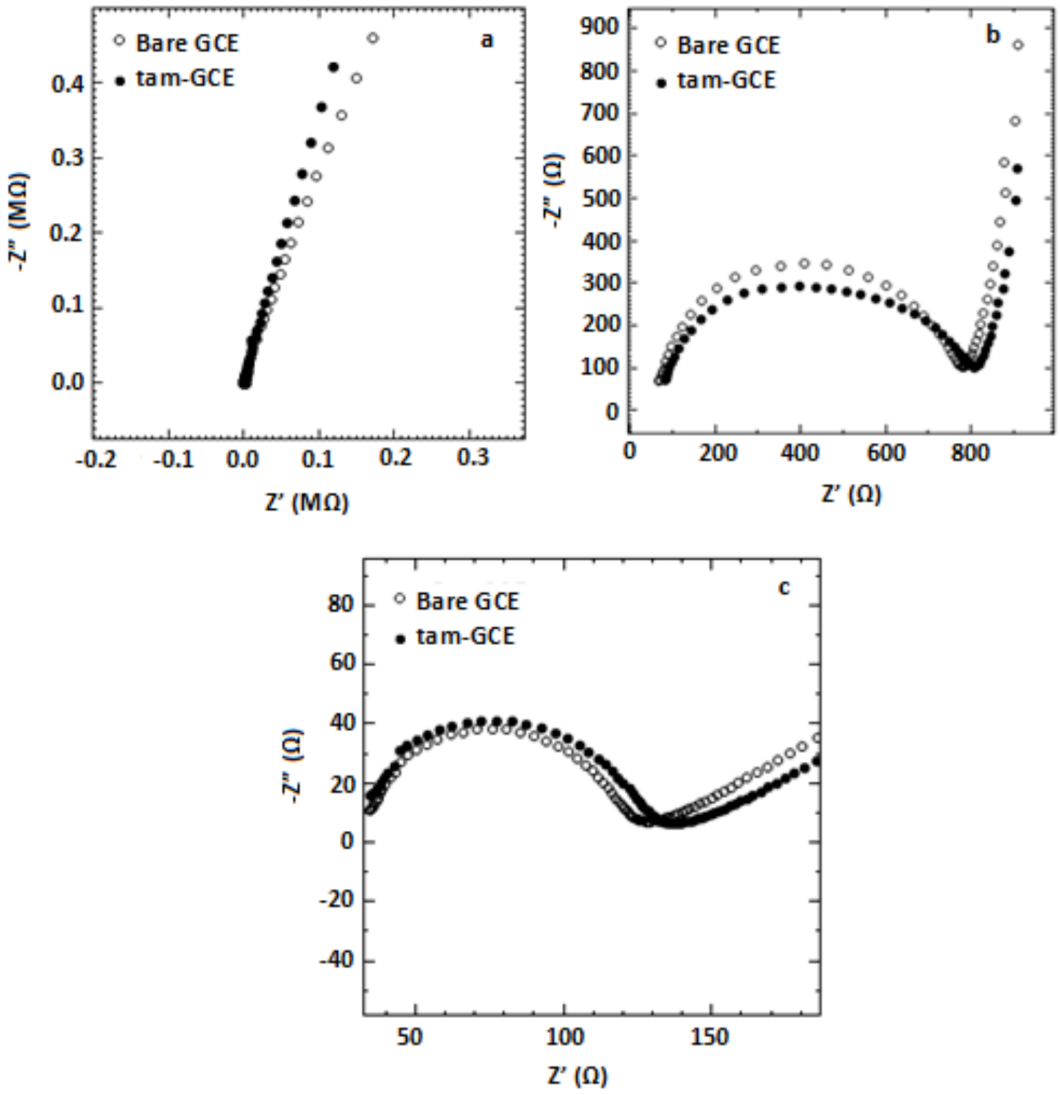

Figure 7. Nyquist plots of bare (o) and tam-covered GCE (?) in acetate buffer (pH 4) for all (a) an high-frequency (b) regions, and in 0.2 mol L^{-1} NaOH containing 0.05 mol L^{-1} $[Fe(CN)_6]^{-3/-4}$ (c). Frequency range = 10^5 to 0.1 Hz, AC amplitude = 0.1 V.

2.3.3. Effects of the deposition potential

The deposition potential varied from 0.8 to –2 V. The obtained voltammograms and the current peak versus the deposition potential (inset) are shown in Figure 10. As shown, the highest peak resulted from a deposition potential of –0.4 V. As the deposition potential shifted to more positive values, the current peak decreased, because the tam is better adsorbed in a negative potential compared to the more positive potentials.[35] In addition, the current peak was decreased by diminishing the deposition potential to more negative values ($<-$ 0.4 V). This is because the hydrogen evolution reaction was accelerated in these potentials and suppressed the adsorbing of the tam analyte. Based on these results, an adsorptive process predominantly contributes to the DPAV of tam. Hence, a deposition potential of –0.4 V was selected as the optimal value for the next experiments.

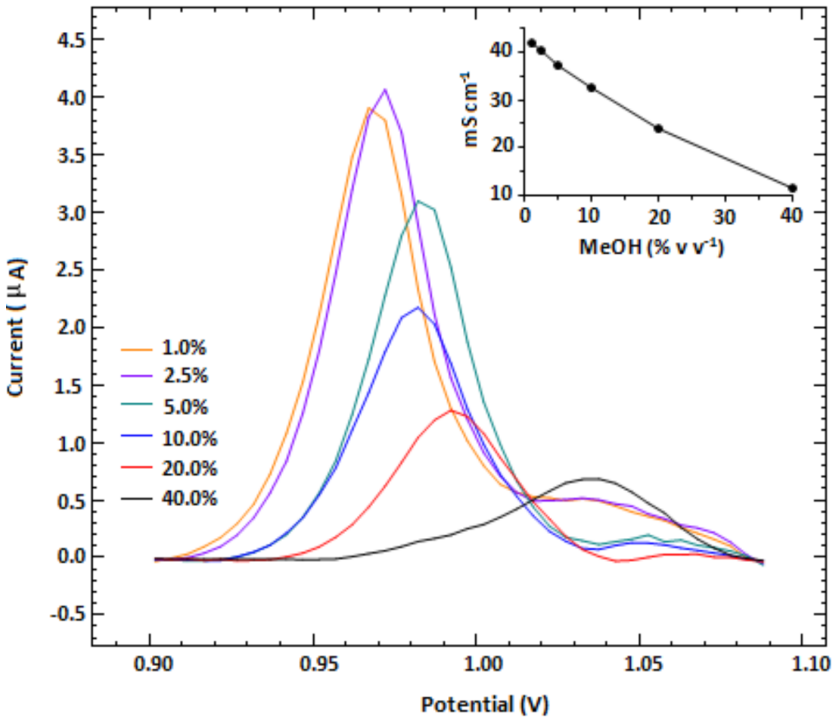

Figure 8. Effects of MeOH content on the peak height of tam oxidation and the plot of specific conductivity versus MeOH content (inset).

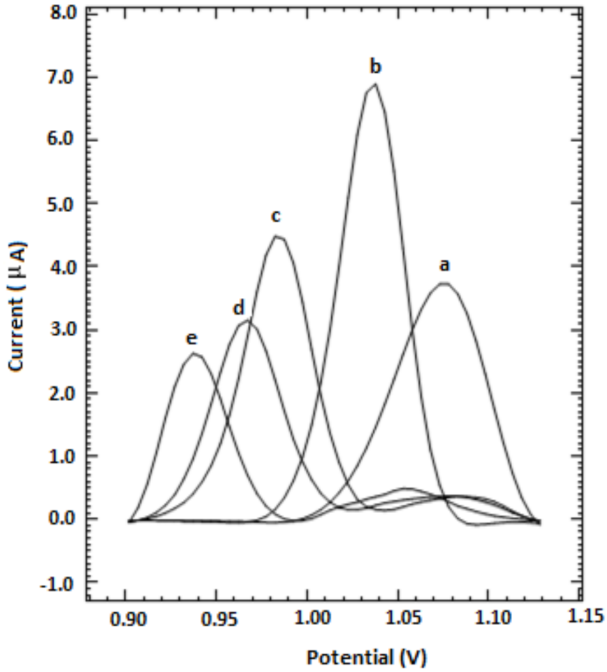

Figure 9. DPAV of 5 μg mL^{-1} tam in 0.01(a), 0.1(b), 0.5 (c), 1 (d), and 2(e) mol L^{-1} H_2SO_4:2.5% v v^{-1} MeOH.

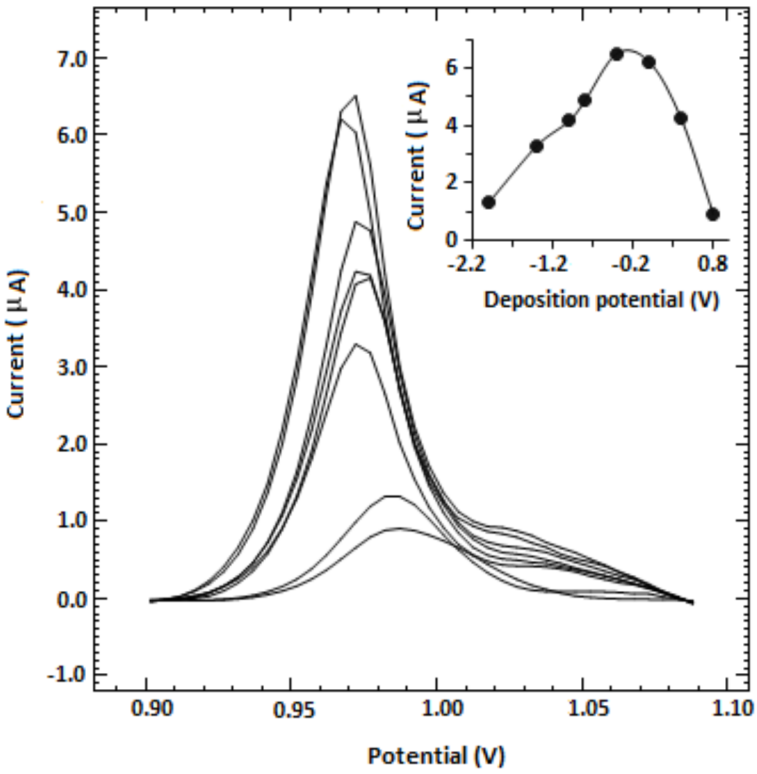

Figure 10. Obtained DPAV at different deposition potential and the plot of the current peak versus the deposition potential (inset).

2.3.4. Effects of the deposition time and rotation rate

The effect of the electrolysis time in –0.4 V vs. Ag/AgCl at the peak high was investigated in the range of 0 to 180 s. The obtained voltammograms and the current peak versus the deposition time (inset) are shown in Figure 11 and show that the best signal was achieved after 30 s of cathodic adsorptive deposition. This is because, at longer deposition times, the hydrogen gas evolution caused the tam-deposited layer to be destroyed and the signal strength in the DPAV step to be diminished. Therefore, this study suggests that the electrochemical adsorption equilibrium for tam is achieved after 30 s electrolysis in –0.4 V. Thus, this time was chosen to perform the next experiments. The effect of the rotation rate was also investigated from 0 to 4000 rpm. The obtained voltammograms and the peak height versus the rpm (inset) are presented in Figure 12. The dependence of the peak height on the rotation rate did not follow a uniform increasing or decreasing trend. The highest peak was achieved by 400 rpm, which was selected as the optimal value.

2.4. Calibration of the proposed method and merit figures

Under the optimum conditions achieved in the optimization section, the proposed method was calibrated in the concentration range of 0.5 to 5 μg mL^{-1} (Figure 13). The calibration plot (Figure 13, inset) was found to be linear for the working concentration range. The following equation presents a good correlation coefficient:

$$I_P = 1.5028C_{Tam} - 0.1205r^2 = 0.9978, \tag{5}$$

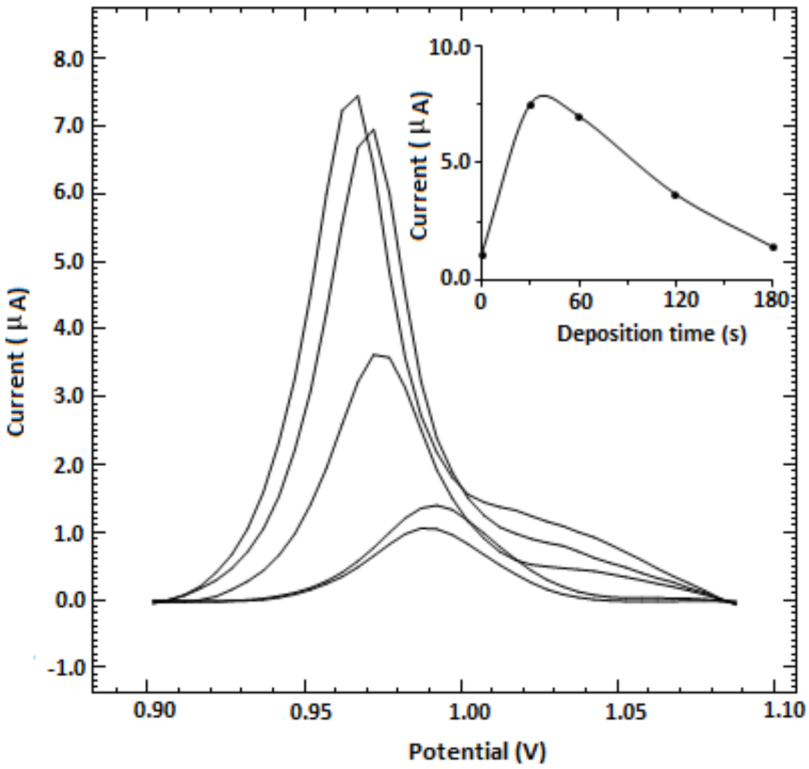

Figure 11. Obtained DPAV at different deposition times and the plot of the current peak versus the time (inset).

where I_P is the tam oxidation current peak (after the background correction) and C_{Tam} is the amount of tam in μg mL^{-1}. The limit of detection is given by LOD = $3S_d/m$, where S_d is the standard deviation of 5 replicates of blank and m is the slope of the calibration plot. Hence, the value of the LOD was 0.008 μg mL^{-1}. The lowest level of the analyte, or the limit of quantitation (LOQ = $10S_d/m$) that can be measured by this method, was 0.025 μg mL^{-1}.

To estimate the accuracy and precision of the proposed method, a standard solution of tam, 2 μg mL^{-1} in 0.1 mol L^{-1} H_2SO_4:2.5% v v^{-1} MeOH, was analyzed 5 times, and the mean, relative bias, and RSD (%) of the method were 1.9 μg mL^{-1}, 5%, and 2.3%, respectively. However, such merit figures represented the proposed method's capability to analyze the tam analyte in an acidic aqueous solution.

2.5. Pharmaceutical application and validation of the proposed method

To apply the suggested method, the extraction of tam from the powdered commercial tablets containing 20 mg of tam citrate was optimized. The best conditions for extracting 96% of the tam were as follows: 6 mL of MeOH and 5 min of stirring at 350 rpm. Using DPAV, the tam citrate-containing analytical samples with concentration levels in the range of the calibration plot were prepared by dilution of the extracted samples in 10 mL of H_2SO_4 0.1 mol L^{-1}:2.5 % v v^{-1} MeOH. Therefore, the content of the tam citrate in the powdered tablets was found to be 19.1 mg, which confirms the relative bias of the method.

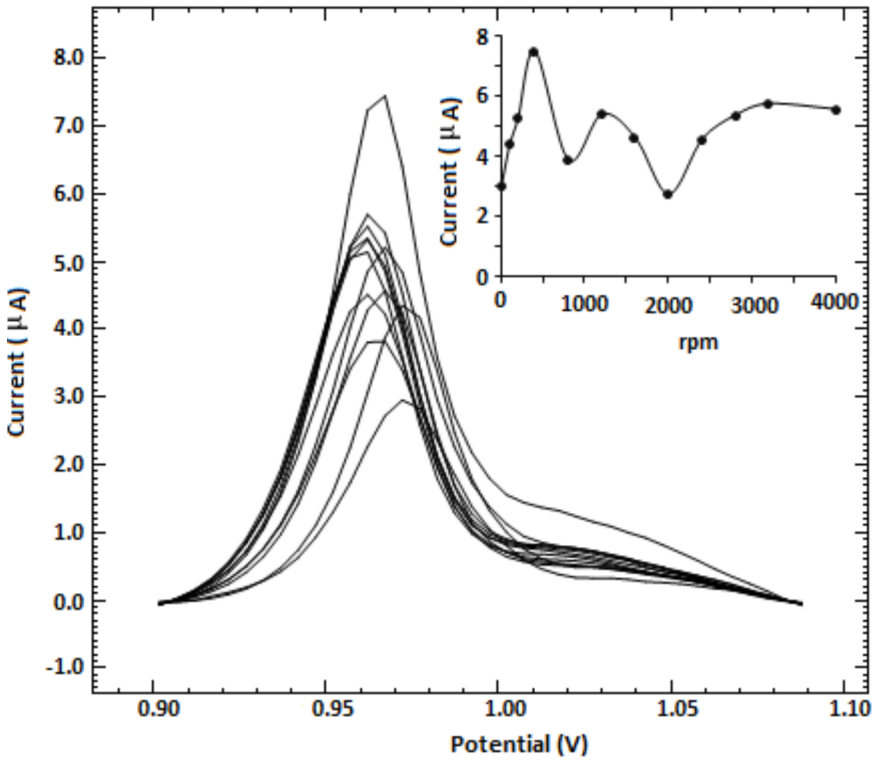

Figure 12. Obtained DPAV at different rotation rates of the GCE and the plot of the peak height versus the rpm (inset).

2.6. Application of the proposed method in serum analysis

To check the capability of the proposed DPAV to analyze tam-spiked human blood serum, optimal conditions were employed after the sample preparation. As pointed out in the literature,[41] more than 99% of tam molecules are strongly bound to serum proteins. Therefore, this strong bond must be broken to prevent the interfering effects of serum proteins. To investigate the effect of this binding on tam electrochemical oxidation, the DPAV of 5 μg mL^{-1} tam was recorded in 10 mL of 0.1 mol L^{-1} H_2SO_4:2.5% v v^{-1} MeOH containing 1 mL of serum (i.e. the blank sample, Figure 14). The tam–protein interaction caused the tam oxidation peak to disappear. However, in another experiment, the tam–protein bond was broken by addition of 2 mL of CH_3CN;[42] subsequently, the precipitated proteins were centrifuged and the supernatant phase was used to perform the DPAV. As shown in Figure 14, the tam oxidation peak appeared after the precipitation and separation of the serum proteins. Thus, to apply the proposed method in order to measure the level of tam in blood, the isolation of serum proteins using CH_3CN is necessary. However, three tam-spiked serum samples with different concentrations of tam (i.e. 3, 4, and 8 μg mL^{-1}) were prepared and then employed to separate the serum proteins in accordance with sec. 3.6. Subsequently, the DPAVs were performed, and the tam concentration was obtained by calibration curve and dilution calculations. The results and recovery percentage are presented in Table 1. As shown in Table 1, the correction factor of the proposed method for analyzing the tam in the serum samples was approximately 1.17.

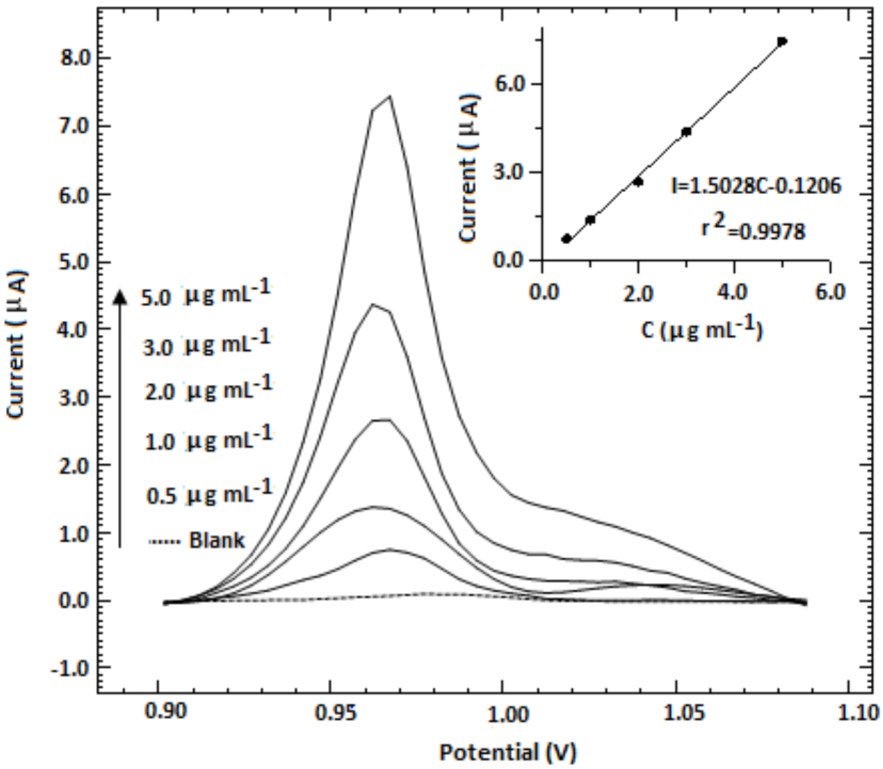

Figure 13. Obtained DPAV of different standards of tam and the corresponding calibration plot (inset) under optimal conditions.

Table 1. The analysis of serum samples spiked with different concentration of tam.

Serum sample	Tam^a (μg mL^{-1})	Tam^b (μg mL^{-1})	Recovery (%)
1	0	ND	0
2	3	2.56	85.3
3	4	3.42	85.5
4	8	6.88	86.0

a) Tam concentration in spiked serum samples.
b) Tam concentration in 10 mL of the prepared analytical samples.

2.7. Comparison with other reported methods

The analytical characteristics of the proposed methods, including LOD, LOQ, and RSD (%), were compared with other methods, as shown in Table 2. As presented in this comparison, the merit figures of this method are better than some others. However, the DPAV methodology is both qualitatively and quantitatively reliable for pharmaceutical and serological analyses.

3. Experimental setup

3.1. Chemicals

All chemicals used were analytical reagent-grade quality and were employed without further purification. The tam citrate was purchased from Sigma-Aldrich. The tablets containing tam, labeled "20 mg tam citrate", were purchased from commercial sources. The other common chemicals, including CH_3CN, CH_3OH, H_2SO_4, HCl,

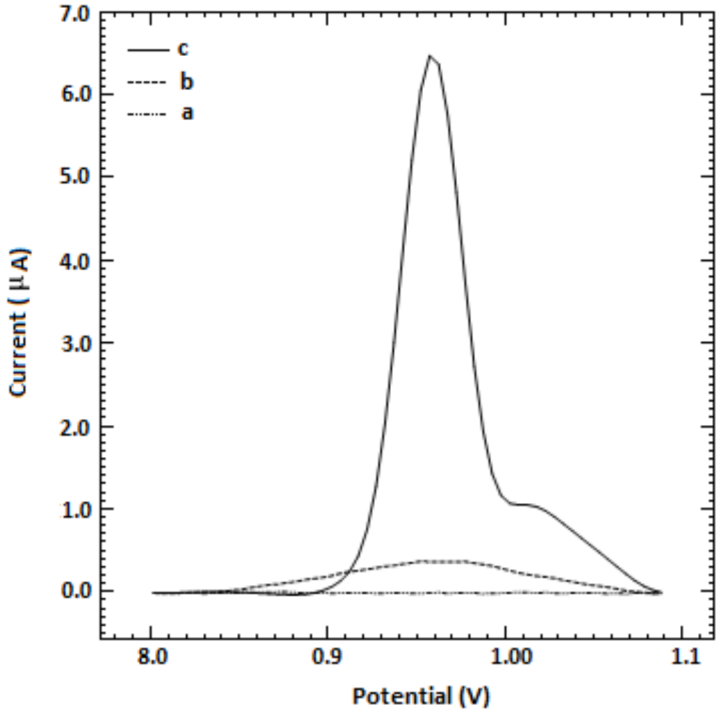

Figure 14. DPAV of 10 mL of 0.1 mol L^{-1} H_2SO_4:2.5% v v^{-1} MeOH containing 1 mL of serum as blank (a), 10 mL of 5 μg mL^{-1} tam in the blank (b), and the b sample after isolating the serum proteins (c).

Table 2. Comparison with other methods.

Method	LOD (μg mL^{-1})	LOQ (μg mL^{-1})	RSD (%)
Square-wave adsorptive anodic stripping voltammetry[35]	0.090	0.29	-
Molecule imprinting-chemiluminescence[43]	0.040	0.13	4.1
Micellar liquid chromatography[44]	0.065	0.17	< 9.2
Nonaqueous capillary zone electrophoresis (NACE)[45]	0.003	0.01	2.8
Capillary gas chromatographic[46]	0.006	0.02	3.6
Spectrophotometric[47]	0.373	1.13	1.5
Proposed athod	0.008	0.02	2.3

H_3PO_4, and CH_3COOH, were also analytical grade and purchased from Merck. The MWCNTs (95% purity, OD = 10-30 nm, ID = 5–10 nm and length = 0.5–500 μm) were obtained from Aldrich. The B-R buffer (pH 4.2) was prepared using a solution containing 0.04 mol L^{-1} acetic, orthophosphoric, and boric acids neutralized with 1 mol L^{-1} NaOH to yield the required pH.

3.2. Instruments

A potentiostat/galvanostat, model PGSTAT302N (Metrohm-Autolab, Switzerland), equipped with rotating disk electrode (RDE) and a three-electrode cell was used to record the voltammograms. Ag/AgCl and Pt rods were used as reference and counter electrodes, respectively. Different electrodes, including GC, Au, Pt, MWCNT paste, and MWCNT-GC electrodes, were used as working electrodes. A pH meter, model Metrohm 827 (Switzerland), was used to adjust the pH of the solutions.

3.3. Preparation of the MWCNT paste and MWCNT-GC electrodes

To prepare the MWCNT electrodes, 50 mg of graphite powder was mixed with 10 mg of MWCNTs in a mortar. Then 0.5 g of paraffin was added to the mixture and it was mixed well for 30 min. The uniformly wetted MWCNT paste was packed into an empty GCE body (OD = 3 mm) and the MWCNT paste electrode was prepared. When necessary, a fresh surface was achieved by sputtering the old surface. The MWCNT-modified GCE was prepared by injecting one drop of the MWCNT:MeOH (70% w w^{-1}) containing 0.5% w w^{-1} Nafion polyelectrolyte on the surface of the GCE and subsequently dried at 60 °C for 30 min.

3.4. Analytical procedure

A 10-mL solution containing tam was transferred to an electrochemical cell. Then the deposition of tam was conducted at –0.4 V versus Ag/AgCl in 0.1 mol L^{-1} H_2SO_4:2.5% v v^{-1} MeOH for 30 s at 400 rpm. Then, after 10 s, a differential pulse anodic stripping voltammogram (0–1.4 V) was recorded at a pulse amplitude of 25 mV, pulse intervals of 0.5 s, and a scan rate of 10 mV s^{-1}.

3.5. Extraction of tam from ground tablets

To optimize the extraction of tam from tablets, 10 tablets were weighed and the average mass per tablet was determined. The tablets were then ground to a fine homogeneous powder in a mortar. A portion of the finely ground material equivalent to 20 mg of tam was dissolved in 6 mL of methanol, stirred in a batch process for 5 min, and filtered using filter paper. Next, 0.2 mL of the sample was diluted up to 10 mL of 0.1 mol L^{-1} H_2SO_4:20% v v^{-1} MeOH. Finally, 0.5 mL of the solution was taken and diluted by 0.1 mol L^{-1} H_2SO_4:2.5% v v^{-1} MeOH to obtain a volume of 10 mL. Subsequently, the obtained sample was analyzed by the proposed DPAV and the extraction recovery (ER%) was calculated.

3.6. Preparation of spiked serum samples

The serum samples (5 mL) were spiked by a stock tam solution and 5 mL of nonspiked serum was selected as the blank. The tam-spiked serum samples were shaken for 2 min; subsequently, 5 mL of CH_3CN was added to each tam-spiked serum sample to prevent protein-drug binding. This mixture was vortexed for 10 min and then centrifuged at 4000 rpm to separate the precipitated proteins. Subsequently, the supernatant phase was transferred into a 10-mL flask and the H_2SO_4 concentration was adjusted to 0.1 mol L^{-1} by adding 2 mol L^{-1} H_2SO_4. It was then diluted up to 10 mL with double-distilled water and employed to perform the DPAV experiment.

4. Conclusion

Cyclic voltammetry behavior of tam was examined in different electrolytes on solid state electrodes. The obtained results demonstrated that the best electrolyte and electrode are 0.1 mol L^{-1} H_2SO_4:2.5% v v^{-1} MeOH and GCE, respectively. The electrochemical characterization was also performed by chronoamperometry, DPAV, and EIS. Therefore, a surface-controlled mechanism was suggested for tam oxidation in this electrolyte. As an analytical application, the DPAV of tam in 0.1 mol L^{-1} H_2SO_4:2.5% v v^{-1} MeOH on the GCE was investigated, and the effects of different factors were optimized. The sharpest peak was achieved under these conditions: 2.5% v v^{-1} MeOH, 0.1 mol L^{-1} H_2SO_4, a deposition potential of 0.4 V, a deposition time of 30 s, and a GCE rotating rate of 400 rpm. Then the calibration curve was plotted under optimal conditions. The proposed method presented proper merit figures to analyze the pharmaceutical and serological samples. This measurement method of tam is simple, rapid, inexpensive, and sensitive.

References

1. Jordan, V. C. *Endocr.-Relat. Cancer* **2014**, *21*, R235-R246.
2. Desta, Z.; Ward, B. A.; Soukhova, N.; Flockhart, D. A. *J. Pharmacol. Exp.* **2004**, *310*, 1062-1075.
3. Wang, D. Y.; Fulthorpe, R.; Liss, S. N.; Edwards, E. A. *Mol. Endocrinol.* **2004**, *18*, 402-411.
4. Shang, Y.; Hu, X.; DiRenzo, J.; Lazar, M. A.; Brown, M. *Cell* **2000**, *103*, 843-852.
5. Massarweh, S.; Osborne, C. K., Creighton, C. J.; Qin, L.; Tsimelzon, A.; Huang, S.; Weiss, H.; Rimawi, M.; Schiff, R. *Cancer Res.* **2008**, *68*, 826-833.
6. Hurtado, A.; Holmes, K. A.; Geistlinger, T. R.; Hutcheson, I. R.; Nicholson, R. I.; Brown, M.; Jiang, J.; Howat, W. J.; Ali, S.; Carroll, J. S. *Nature* **2008**, *456*, 663-666.
7. Osborne, C. K.; Bardou, V.; Hopp, T. A.; Chamness, G. C.; Hilsenbeck, S. G.; Fuqua, S. A.; Wong, J.; Allred, D. C.; Clark, G. M.; Schiff, R. *J. Natl. Cancer Inst.* **2003**, *95*, 353-361.
8. Chilukuri Sastry, S. P.; Lingeswara Rao, J. S. V. M.; Rao, K. R. *Talanta* **1995**, *42*, 1479-1485.
9. Sastry, C. S. P.; Lingeswara Rao, J. S. V. M. *Indian J. Pharm. Sci.* **1995**, *57*, 133-135.
10. Browna, S. A.; Akpadioa, E. I.; Akpab, P. A.; Nnamanib, P. O.; Akabuogub, B. C.; Onunkwob, G. C. *Iran. J. Pharm. Sci.* **2007**, *3*, 203-208.
11. Fathima, A.; Rao, S.; Venkateshwarlu, G. *International Journal of ChemTech Research* **2012**, *4*, 79-91.
12. El-Leithy, E. S.; Abdel-Rashid, R. S. *Asian J. Pharm. Sci.* **2016**, *11*, 318-325.
13. Clède, S.; Lambert, F.; Sandt, C.; Gueroui, Z.; Delsuc, N.; Dumas, P.; Vessières, A.; Policar, C. *Biotechnol. Adv.* **2013**, *31*, 393-395.
14. Dicko, A.; Morissette, M.; Ameur, S. B.; Pezolet, M.; Paolo, T. D. *Brain Res. Bull.* **1999**, 401-405.
15. Heath, D. D.; Flatt, S. W.; Wu, A. H. B.; Pruitt, M. A.; Rock, C. L. *Br. J. Biomed. Sci.* **2014**, *71*, 33-39.
16. Antunes, M. V.; Rosa, D. D.; Viana, T. D. S.; Andreolla, H.; Fontanive, T. O.; Linden, R. *J. Pharm. Biomed. Anal.* **2013**, *76*, 13-20.
17. Sane, R. T.; Desai, S. V.; Sonawne, K. K.; Nayak, V. G. *J. Chromatogr. A* **1985**, *331*, 432-436.
18. Daniel, C. P.; Gaskell, S. J.; Bishop, H.; Nicholson, R. I. *J. Endocrinol.* **1979**, *83*, 401-408.
19. Golander, Y.; Sternson, L. A. *J. Chromatogr. B, Biomed. Sci. Appl.* **1980**, *181*, 41-49.
20. Husain, S.; Alvi, S. N.; Rao, R. N. *Anal. Lett.* **1994**, *27*, 2485-2497.
21. Sanders, J. M.; Burka, L. T.; Shelby, M. D.; Newbold, R. R.; Cunningham, M. L. *J. Chromatogr. B, Biomed. Sci. Appl.* **1997**, *695*, 181-185.
22. Thang, L. Y.; See, H. H.; Quirino, J. P. *Electrophoresis* **2016**, *37*, 1166-1169.

23. Thang, L. Y.; Shahir, S.; See, H. H. *Electrophoresis* **2015**, *36*, 2713-2719.
24. Lu, W.; Poon, G. K.; Carmichael, P. L.; Cole, R. B. *Anal. Chem.* **1996**, *68*, 668-674.
25. Flores, J. R.; Nevado, J. J.; Salcedo, A. M.; Díaz, M. P. *Talanta* **2005**, *65*, 155-162.
26. Carter, X. F. Li, S. J.; Dovichi, N. J. *J. Chromatogr. A* **2000**, *895*, 81-85.
27. Brown, R. R.; Bain, R.; Jordan, V. C. *J. Chromatogr. B, Biomed. Appl.* **1983**, *272*, 351-358.
28. Zhu, Y. B.; Zhang, Q.; Zou, J. J.; Yu, C. X., Xiao, D. W. *J. Pharm. Biomed. Anal.* **2008**, *46*, 349-355.
29. Lee, K. H.; Ward, B. A.; Desta, Z.; Flockhart, D.A.; Jones, D. R. *J. Chromatogr. B, Analyt. Technol. Biomed. Life Sci.* **2003**, *791*, 245-253.
30. Stevenson, D.; Briggs, R. J.; Chapman, D. J.; De Vos, D. *J. Pharm. Biomed. Anal.* **1988**, *6*, 1065-1068.
31. Fijalek, Z.; Chodkowski, J.; Warowna, M. *J. Electroanal. Chem.* **1987**, *226*, 129-136.
32. Radhapyari, K.; Kotoky, P.; Khan, R. *Mater. Sci. Eng. C* **2013**, *33*, 583-587.
33. Garrido, J. M. P. J.; Quezada, E.; Fajín, J. L. C.; Cordeir, M. N. D. S.; Garrido, E. M. P. J.; Borges, F. *Int. J. Electrochem. Sci.* **2013**, *8*, 5710 -5723.
34. Yarman, A.; Scheller, F. W. *Sensors* **2014**, *14*, 7647-7654.
35. Sharma, D. K.; Mourya, G. L.; Jhankal, K. K.; Jones, L. A.; Bhargava, S. K. *Der Pharm. Lett.* **2012**, *4*, 1599-1606.
36. Guo, X. X.; Song, Z. J.; Tian, X. J.; Song, J. F. *Anal. Lett.* **2008**, *41*, 1225-1235.
37. Jain, R.; Vikas; Radhapyari, K. *Drug Test. Anal.* **2011**, *3*, 743-747.
38. Oleszczuk, P.; Pan, B.; Xing, B. *Environ. Sci. Technol.* **2009**, *43*, 9167-9173.
39. Laviron, E. *Electroanal. Chem.* **1974**, *52*, 355-393.
40. Lin, K. C.; Jian, X. C.; Chen, S. M. *Int. J. Electrochem. Sci.* **2011**, *6*, 2264-2283.
41. Paterson, S. C.; Lim, C. K.; Smith, K. D. *Biomed. Chrom.* **2003**, *17*, 143-148.
42. Gjerde, J.; Kisanga, E. R.; Hauglid, M.; Holm, P. I.; Mellgren, G.; Lien, E. A. *J. Chromatogr. A* **2005**, *1082*, 6-14.
43. Nle, F.; Lu, J.; He, Y.; Du, J. *Luminescence* **2005**, *20*, 315-320.
44. Peris-Vicente, J.; Ochoa-Aranda, E.; Bose, D.; Esteve-Romero, J. *Talanta* **2015**, *131*, 535-540.
45. Rodrıguez Flores, J.; Berzas Nevado, J. J.; Contento Salcedo, A. M., Cabello Dıa, M. P. *Anal. Chim. Acta* **2004**, *512*, 287-295.
46. Rodrıgue, J.; Berza, J. J.; Content, A. M.; Cabelo, M. P. *J. Sep. Sci.* **2003**, *26*, 915-922.
47. Savitha, R.; Seetama, M.; Yadagiri Swamy, P.; Venkateshwarlu, G. *World Journal of Pharmacy and Pharmaceutical Sciences* **2014**, *4*, 765-773.